Electronic Supplementary Material (ESI) for Chemical Science.

Supplementary Material

Efficiently Self-Healing Boronic Ester Crystals

Patrick Commins,[1] Marieh B. Al-Handawi,[1] Durga Prasad Karothu,[1] Gijo Raj,[1] Panče Naumov[1,2,*]

[1]New York University Abu Dhabi, Abu Dhabi, United Arab Emirates
[2]Radcliffe Institute for Advanced Study, Harvard University, 10 Garden St, Cambridge, MA 02138, USA
Lead contact: pance.naumov@nyu.edu (P. N.)

Experimental Details

Synthesis and characterization of boronic esters 3–6. Compound **3**, **4**, **5** and **6** was prepared using a modified protocol form the literature.[1] All starting materials and chemicals were purchased from Sigma-Aldrich and used without further purification.

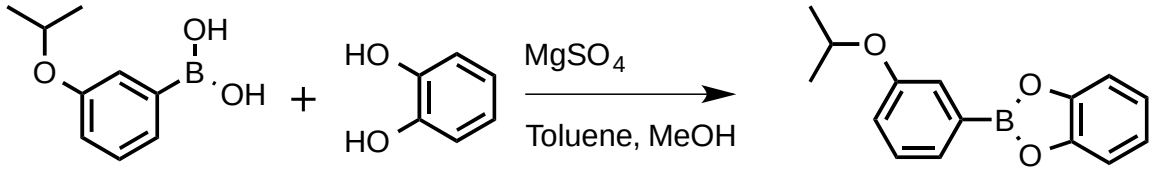

3

Synthesis of the 3-isopropoxyphenylboronic acid catechol ester, 3. Catechol, **2** (1.1 g, 10 mmol), and 3-isopropoxyphenylboronic acid, **1** (1.8 g, 10 mmol) were added to a round-bottom flask containing magnesium sulfate (150 mg, 1.3 mmol) and toluene (25 mL). The reaction was stirred and heated under reflux for 24 h. The resulting suspension was filtered and evaporated using a rotary evaporator. The residue was recrystallized from *n*-hexane to obtain 508 mg of thin translucent crystals (20% yield). Characterization: m.p. 49–51° C. ^{1}H NMR (500 MHz, $CDCl_3$) δ/ppm: 7.64 (d, J = 7.0 Hz, 1H), 7.60 (d, J = 2.0 Hz, 1H), 7.38 (dd, J = 8, 7.5 Hz, 1H), 7.30 (m, 2H), 7.11 (m, 2H), 7.09 (ddd, J = 8.0, 2.5, 1 Hz, 1H) 4.64 (septet, J = 6.0 Hz, 1H), 1.37 (d, J = 6.0 Hz, 6H), ^{13}C NMR (125 MHz, DMSO-d_6) δ/ppm: 157.2, 145. 2, 129.4, 126.6, 121.1, 120.1, 118.3, 116.0, 69.4, 22.2. The carbon adjacent to boron was not detected IR (solid, ATR, cm^{-1}): 3070, 2987, 2973, 2929, 2881, 1567, 1471, 1425, 1369, 1290, 1241, 1216, 1132, 1116, 1064, 997, 970, 809, 742, 700. HRMS (APCI-TOF) calculated for $C_{15}H_{15}B_1O_3$ $[M+H]^+$ m/z = 255.1187, found: 255.1193.

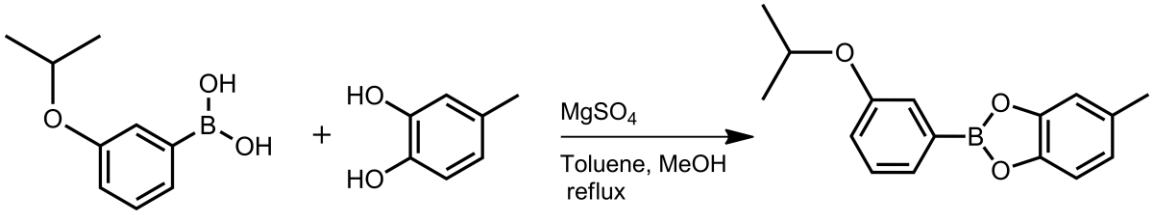

4

Synthesis of the 3-isopropoxyphenylboronic acid 4-methylcatechol ester, 4. 4-Methylcatechol (630 mg, 5 mmol) and 3-isopropoxyphenyl boronic acid (900 mg, 5 mmol) were added to a round-bottom flask containing magnesium sulfate (150 mg, 1.3 mmol), toluene (25 mL) and methanol (2.5 mL). The reaction was stirred and heated to reflux for 24 h. The resulting suspension was filtered and diluted with dichloromethane (20 mL). The organic phase was washed with water (5 mL), and evaporated using a rotary evaporator. The off-white powder was recrystallized from *n*-hexane to obtain 576 mg (43% yield) of translucent needles.

Characterization: m.p. 59–61 °C. ^{1}H NMR (500 MHz, $CDCl_3$) δ/ppm: 7.65 (dd, J = 7.5, 1, Hz, 1H), 7.61 (d, J = 2.5 Hz), 7.40 (apparent triplet, J = 8 Hz, 1H), 7.19 (d, J = 8 Hz), 7.15 (d, J = 1 Hz, 1H), 7.11 (ddd, J = 8.0, 2.5, 1 Hz, 1H), 4.66 (septet, J = 6 Hz), 2.44 (s, 3H), 1.40 (d, J = 6 Hz). ^{13}C NMR (125 MHz, $CDCl_3$) δ/ppm: 157.7, 148.5, 146.4, 132.7, 129.6, 127.2, 123.1, 121.3, 120.7, 113.2, 111.8, 70.0, 22.1, 21.4. The carbon adjacent to boron was not detected. IR (solid, ATR, cm^{-1}): 3070, 2985, 2967, 2925, 2867, 1569, 1492, 1425, 1382, 1359, 1319, 1286, 1236, 1214, 1164, 1137, 1116, 1093, 1064, 997, 968, 881, 821, 802, 700, 670. HRMS (APCI-TOF) calculated for $C_{16}H_{17}B_1O_3$ $[M+H]^+$ m/z: 269.1344, found: 269.1340.

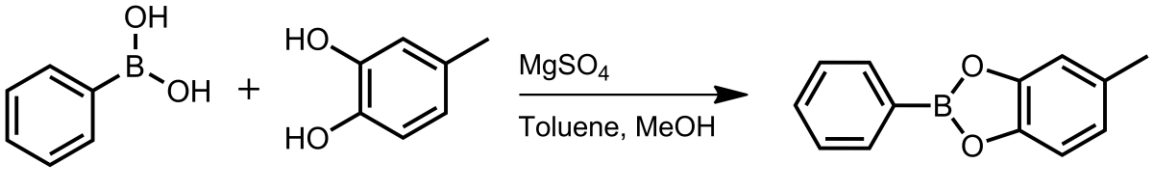

5

Synthesis of the phenylboronic acid 4-methylcatechol ester, 5. 4-Methycatechol (1.24 g, 10 mmol) and phenylboronic acid (1.22 g, 10 mmol) were added to a round-bottom flask containing magnesium sulfate (150 mg, 1.3 mmol), toluene (25 mL), and methanol. The reaction was stirred under reflux for 24 h. The resulting suspension was filtered and evaporated using a rotary evaporator. The residue was recrystallized from toluene to obtain 1662 mg (79% yield) of a transparent hexagonal polycrystalline powder. Characterization: m.p. 117–119 °C. ^{1}H NMR (500 MHz, $CDCl_3$) δ/ppm: 8.11 (m, 2H), 7.58 (m, 2H), 7.50 (m, 1H), 7.21 (m, 2H), 7.16 (s, 1H) 6.96 (d, J = 8.0 Hz, 1H), 2.44 (s, 3H). ^{13}C NMR (125 MHz, $CDCl_3$) δ/ppm: 148.6, 146.4, 135.0, 132.7, 132.3, 128.2, 123.1, 113.2, 111.8, 21.4. The carbon adjacent to boron was not detected. IR (solid, ATR, cm^{-1}) 3050, 3048, 2917, 2863, 1598, 1490, 1484, 1436, 1394, 1361, 1340, 1319, 1255, 1234, 1164, 1068, 1022, 929, 877, 852, 823, 802, 761, 748, 692, 669, 649. HRMS (APCI-TOF) calculated for $C_{13}H_{11}B_1O_2$ $[M+H]^+$ m/z: 211.0925, found: 211.0921.

X-ray powder diffraction. A Panalytical Empyrean system was used for the powder X-ray diffraction measurements using copper as a source (1.5418 Å) at power settings of 45 kV and 40 mA. The beam passed through a programmable slit that illuminated the powder sample at 0.5°. The diffracted beam was measured using a Pixcel solid-state detector with a beta filter and a resolution of 0.0134°. Grinding experiments were performed by sequentially grinding the material for set durations and then immediately acquiring the diffraction pattern.

Single crystal X-ray diffraction. Crystals obtained from *n*-hexane were measured and exhibited diffracted with discrete diffraction pattern that confirms it is a single crystal, but diffracted poorly at higher angles. Although the structure was determined, due to the weak reflections at high angles, the structure could be refined only to *R* factor of 11%. Instead, single crystals of sufficient quality were acquired by *in situ* crystallization using an optical heating crystallization device

(OHCD).[2] The method used a crystal of **3** of poor diffraction quality, which was alternatively melted by an infrared laser and cooled inside a glass capillary until a crystal of sufficient quality was obtained (Fig. S1). The crystal habits for the crystals obtained by slow evaporation from *n*-hexane and OHCD were identical. Both crystals had discrete diffraction patterns and were crystalline (Fig. S1). The crystals were placed in a 1.5-mm diameter glass capillary (~20 mm length), sealed at both ends using cyanoacrylate glue, and attached to a goniometer head. The goniometer head was mounted on a diffractometer equipped with a low-temperature device and OHCD for laser-assisted melting (CO_2 laser, λ = 10.6 μm). The capillary was cooled to –173.15 °C. A solid-to-melt equilibrium was established in a narrow zone of the capillary by heating with the laser (20% laser power), where a new colorless, block-shaped crystal was grown in the capillary over a duration of 4 hours. This capillary was carefully removed from the diffractometer and cut to separate the crystal. This crystal was used for the single crystal X-ray diffraction analysis by using a Apex DUO diffractometer (Bruker), using graphite-monochromated Mo K_α radiation (λ = 0.71073 Å) and CCD as area detector at –173.15 °C. Bruker's Apex II software[3] was used for the unit cell measurements, data collection, integration, scaling and absorption corrections. The diffraction images were integrated by using Bruker's SAINT program.[4] Multi-scan absorption corrections were applied to the data by using SADABS.[5] The structure was solved by direct methods using SHELXS97[5] and refined by full-matrix least-squares methods based on F^2 using SHELXL97 within the program suite WinGX.[6] All non-hydrogen atoms were refined anisotropically, hydrogen atoms bonded to carbon atoms were fixed using the HFIX command in SHELX-TL.[7] A check of the final CIF using PLATON as part of WinGX[6,8] did not show any missing symmetry. Geometrical calculations were done using PLATON[8] and PARST.[9] The packing diagrams were generated using Mercury 3.7.[10] Additional details of the data collections and structural refinement parameters are provided in Supporting Table S1.

Nuclear magnetic resonance (NMR) spectroscopy. The spectra were recorded at 25 °C on a 500 MHz Bruker Avance 500 spectrometer for the ^{1}H nuclei and 125 MHz for the ^{13}C NMR. The chemical shifts are reported in ppm relative to the signals corresponding to the residual non-deuterated solvent (DMSO-d_6, 2.50 ppm; $CDCl_3$, 7.28 ppm).

Computerized tomography (CT). The 3D CT scans were acquired on an X View CT Scanner, X500 CT. The scans were acquired with a working voltage of 160 kV and 100 A. The crystals were mounted on a molding clay and scanned at a rate of 7.5 frames per second. The images were processed and videos were recorded using X View CT's default software, eFX-view. In the CT images, the density of the material is represented by its color.

Tensile and three-point bending measurements. Tensile and three-point bending measurements were performed on MTII/Fullam Semtester tensile tester (MTI Instruments) equipped with a 50 lbs for the tensile measurements and a 5 N load cell for the three-point bending measurements. For the tensile measurement,

the crystals were attached to a pair of silicone pads using a minimal amount of two-component super-glue (Araldite). The crystal was separated using the tensile tester's decompression mode and subsequently compressed in compression mode using approximately 0.5–1 N of force for 24 hours at 22 °C and ambient humidity (37% RH). The healed crystal was decompressed at a rate of 0.005 mm/s until the two crystals were visibly separated. The tensile strength of the crystal was determined by measuring the drop in the load at the break point normalized by the cross-sectional area in between the two interfaces. The surface area of the healed interface was measured by approximating the surface as a rectangle and measuring the dimensions using SEM. Immediately after decompression of the healed interface, the two faces were compressed to their original positions, held for 5 seconds, and the tensile strength of the material was measured as described above. The three-point bending measurements were performed by placing the crystal on the stage with a 2.1 mm span distance and had the jig approach the crystal at 0.05 mm/s. The following equations were used:

$$\text{Strain} = \frac{6 * \Delta D * \text{height}}{L^2}$$

$$\text{Stress} = \frac{3 * \text{force} * L}{2 * \text{width} * \text{height}^2}$$

$$\text{Elastic Modulus} = \frac{\text{Stress}}{\text{Strain}}$$

Where L is the span between the two supports, ΔD is the change in displacement, force is the measured force from the tensile tester, height is the thickness of the crystal, and width is the width of the crystal.

Optical microscopy and images. The optical images were acquired using either a camera within a cell phone iPhone6, a Nikon SMZ1500 microscope equipped with a camera Nikon Coolpix P7800, or a Sony Alpha Mark II (ILCE-7RM2) camera. Images were processed for increased clarity using Adobe Photoshop CC 2014 by applying global changes such as brightness and contrast adjustments.

Scanning electron microscopy (SEM). The SEM experiments were conducted under high vacuum with a QUANTA FEG 450 electron microscope with a primary electron energy of 1–3 kV. The twisting and untwisting experiments were accomplished by twisting a crystal manually using forceps and adhering the twisted end to a piece of carbon tape. The crystal was then removed from the tape and untwisted. The bent crystal images were acquired by adhering one end to the carbon tape and bending the free hanging end using a pair of forceps. The crystal was then unbent by pulling the free end of the crystal and straightening it.

Atomic force microscopy (AFM). AFM was performed on a combined WItec alpha 300 system in ac ("tapping") mode. The cantilevers were operated at resonance frequency of 204–497 kHz and with a nominal tip radius of 15 nm. A 10 × 10 μm area was initially imaged and the surface was continually scanned for 18.5

hours at 22 ^{o}C and 37% relative humidity. All images were processed and analyzed using the Gwyddion software.[11]

Fabrication of AFM crystal probes. The AFM crystal probes were fabricated by gluing a small (190 × 160 μm) piece of a flat crystal over a tipless AFM cantilever (Model, TL-FM, NanoAndMore USA). The tipless cantilever was initially held using hooked tweezers (Ted Pella, code: 5624) and focused under an optical microscope (Nikon) having sufficiently large working distance. A tiny quantity of a two-component epoxy glue (Loctite EA3430) was placed on the extremity of the AFM cantilever using a small piece of cleaned hair, and fastened between a pair of auto-locking tweezers (Ted Pella, code 5372 NM). A flat edged single crystal was carefully picked using another set of hair-fastened tweezers, and was placed over the glue at the extreme end of the cantilever. The crystal-glued cantilever was allowed to dry and cure inside a desiccator for 24 hours.

AFM force measurements. The force-distance curves were recorded using a commercial AFM (Dimension Icon, Bruker Nanosurfaces). The deflection sensitivity of the crystal probe (279.3 nm/V) is first measured by performing several force-distance ramps on a standard sapphire sample (sapphire-12M). After withdrawing several micrometers away from the surface, the spring constant of the crystal probe was determined by the thermal tuning method integrated in the Bruker Nanoscope image acquisition software. Once the deflection sensitivity and the spring constant of the crystal probe was calibrated, force measurement was performed on a flat crystal sample fixed onto standard AFM sample support steel disc (Ted Pella 16028, 0.12 mm). Quantitative analysis of the force-distance curves was performed using the SPIP software (Image Metrology A/S, Denmark).

Attenuated total reflectance infrared microscopy (AFM). ATR-IR spectra were acquired on a Agilent Cary 600 Series FTIR spectrometer. The scans were carried out from 4000–800 cm^{-1}.

Supporting References

1. A. D. Herrera-España, G. Campillo-Alvarado, P. Román-Bravo, D. Herrera-Ruiz, H. Höpfl, H. Morales-Rojas, *Cryst. Growth Des.* 2015, **15**, 1572–1576.

2. R. Boese, M. Nussbaumer, *In situ Crystallization Techniques. In Correlations, Transformations, and Interactions in Organic Crystal Chemistry.* IUCr Crystallographic Symposia. (Jones, D. W., Katrusiak, A. Eds.), Oxford University Press, Oxford, England, **1994** pp. 20–37.

3. *APEX DUO*, version 2.1–4; SAINT, version 7.34A (Bruker AXS Inc., 2012).

4. *Bruker 2006b. SAINT*, Version 7.60a. (Bruker AXS Inc.) Madison, Wisconsin, USA.

5. *Bruker 2006a. SADABS*, Version 2.05. (Bruker AXS Inc.) Madison, Wisconsin, USA.

6. L. J. Farrugia, WinGX and ORTEP for Windows: an update. *J. Appl. Cryst.* **2012**, *45*, 849–854.

7. G. M. A. Sheldrick, *Acta Crystallogr. A*. 2008, **64**, 112–122.

8. A. L. Spek, J. Appl. Cryst. 2003, **36**, 7–13.

9. M. J. Nardelli, Appl. Cryst. 1995, **28**, 659.

10. C. F. Macrae, I. J. Bruno, J. A. Chisholm, P. R. Edgington, P. McCabe, E. Pidcock, L. Rodriguez-Monge, R. Taylor, J. van de Streek, P. A. Wood, *J. Appl. Cryst.* 2008, **41**, 466–470.

11. D. Nečas, P. Klapetek, *Cent. Eur. J. Phys.* 2012, **10**, 181–188.

Supplementary Figures

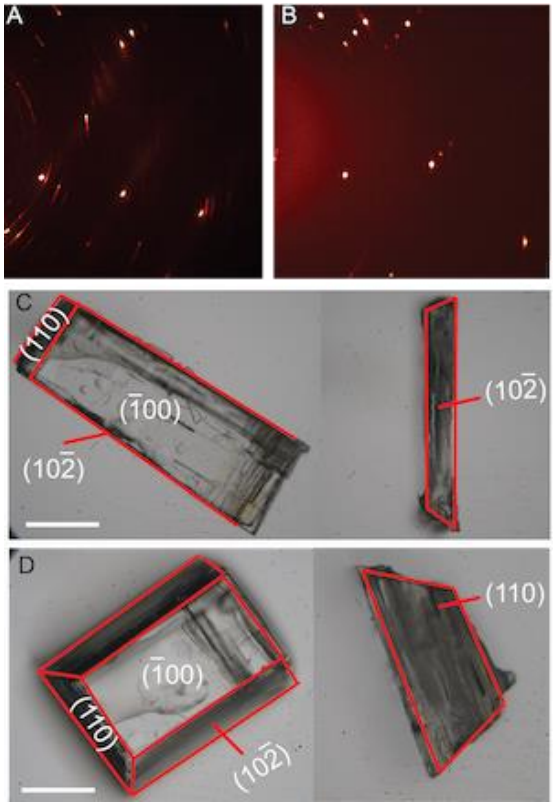

Fig. S1 X-ray diffraction pattern of and face indexing of crystals of **3** grown from *n*-hexane and by using an Optical Heating and Crystallization Device, OHCD. Diffraction image of a crystal grown from *n*-hexane (A) and a crystal grown by OHCD (B). Face indexing of a crystal grown from *n*-hexane (C) and grown by OHCD (D). The habit and crystal faces of the crystal grown from OHCD are the same as those found using slow evaporation. Scale bar: C, 100 μm; D, 10 μm.

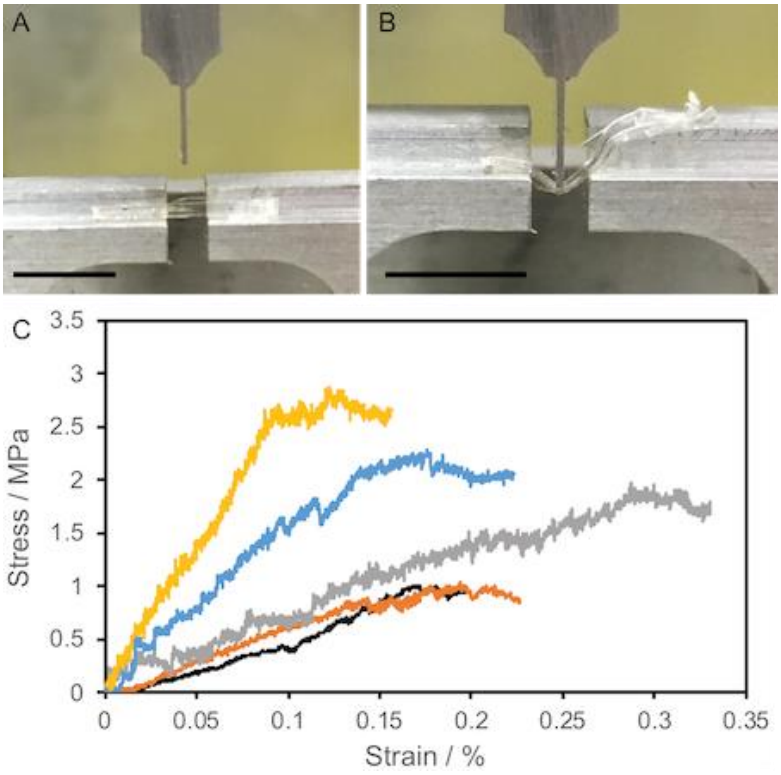

Fig. S2 Three-point bending experiments. Images of the three-point bending experiments before (A) and after (B) bending on the (100) face of a crystal of **3**. (C) Stress-stain curves of five crystals of **3** from three-point bending experiments on the (100) face. The crystals have a range of elastic moduli of 4.8 to 27.2 MPa. The elastic moduli are shown in Table S1. Scale bar, 1 mm.

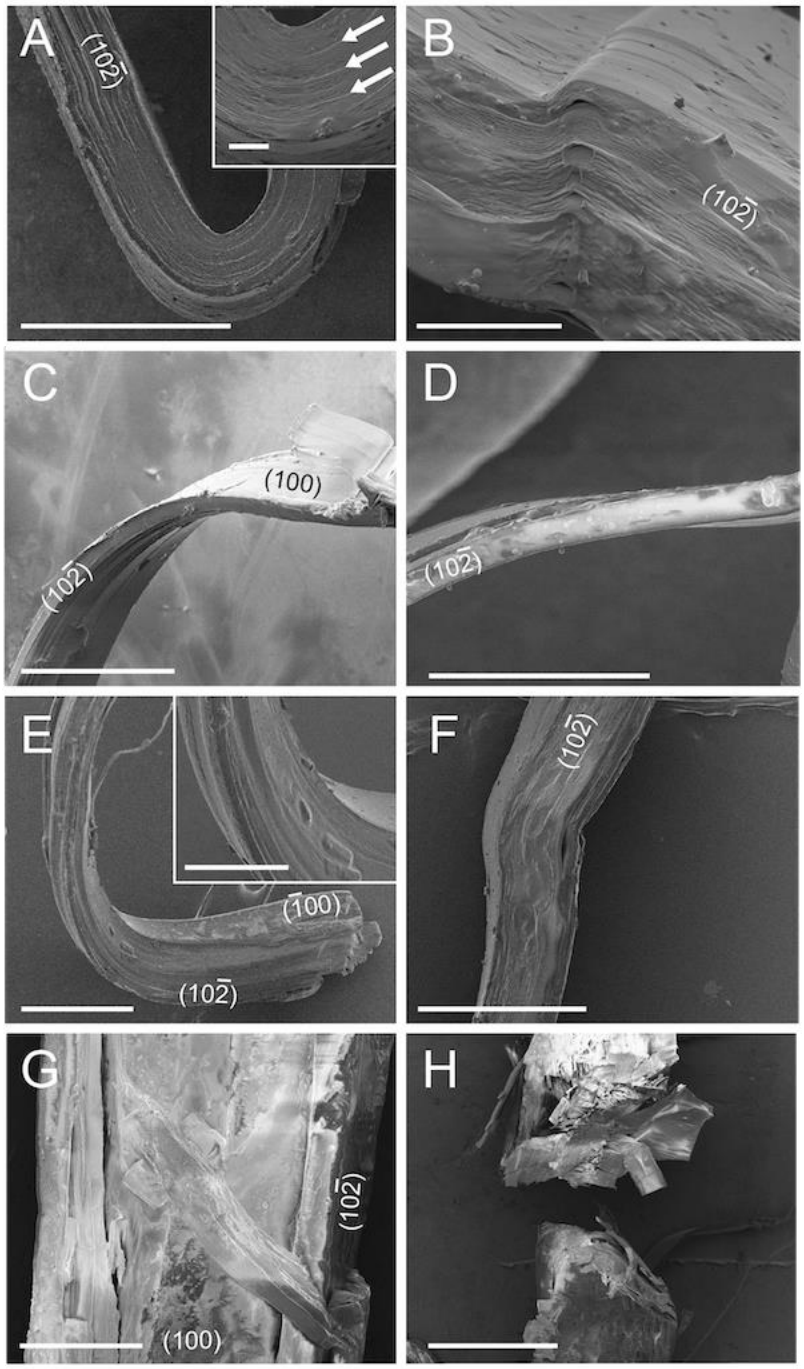

Fig. S3 Scanning electron microscopy images of crystals of **3.** A crystal is bent on its flat face (100), (A). The arrows in the inset in panel A show striations that define the major slabs. A crystal that was unbent and rippled in response (B). When the crystal is twisted (C) it responds elastically and after the removal of the pressure it untwists (D), The crystal coiled (E) and uncoiled (F), and the deformation is plastic due to delamination. When force is applied to the (10 $\bar{2}$) face, the crystal breaks (G and H). Scale bars, A, 500 μm. (inset, 50 μm); B, 100 μm; C, 1 μm; D, 500 μm; E, 500 μm, (inset, 200 μm); F, 500 μm; G, 400 μm; H, 1 μm.

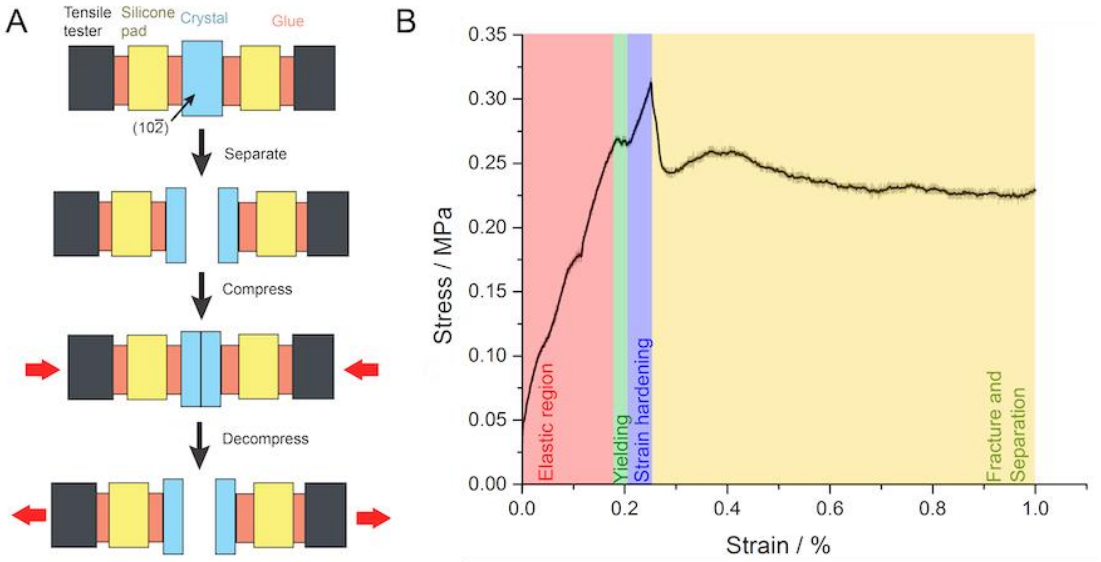

Fig. S4 Tensile setup and mechanicals properties for the virgin break of a crystal of **3**. (A) A cartoon representation of the process used to measure the degree of adhesion and self-healing of a crystal of **3**. (B) A stress-strain curve for the virgin break of **3**. The breakpoint at 0.25 % strain is sharp and corresponds to the crystal separating with a pressure of 0.32 MPa. The Young's modulus was determined from the elastic region of the sample from 0–0.17 % strain to be 1.18 MPa. The error is represented by the shaded region.

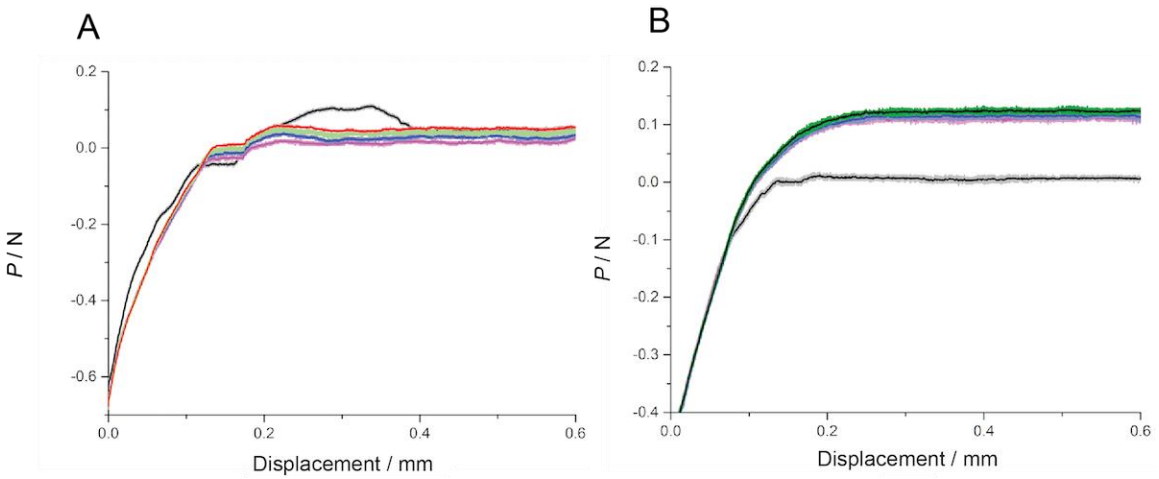

Fig. S5 Recompression experiments for a crystal of **3** that did and did not heal. (A)The breakpoint of the healed crystal was visible at 0.35 mm (black line). The sample was then immediately compressed for 5 s, and then decompressed, and the adhesion was measured (the red, blue, green and magenta lines correspond to four consecutive measurements). There was no adhesion detected. (B) Tensile testing on a crystal that did not show adhesion. The magenta, blue and green lines are recompressions and the initial decompression is shown in black. The error is represented by the shaded regions.

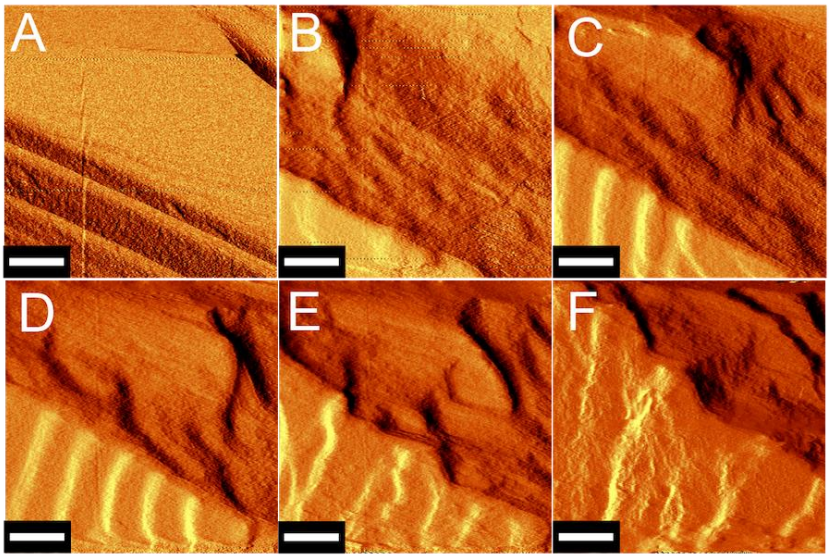

Fig. S6 Atomic force microscopy of the surface of **3** over 18.5 h**.** (A–F) Sequential atomic force microscopy images of the surface of 3 recorded at 0 (D), 3.5 (e), 7.25 (F), 10.25 (G), 13.25 (H) and 17 h (I), respectively. Scale bars, A–F, 2 μm.

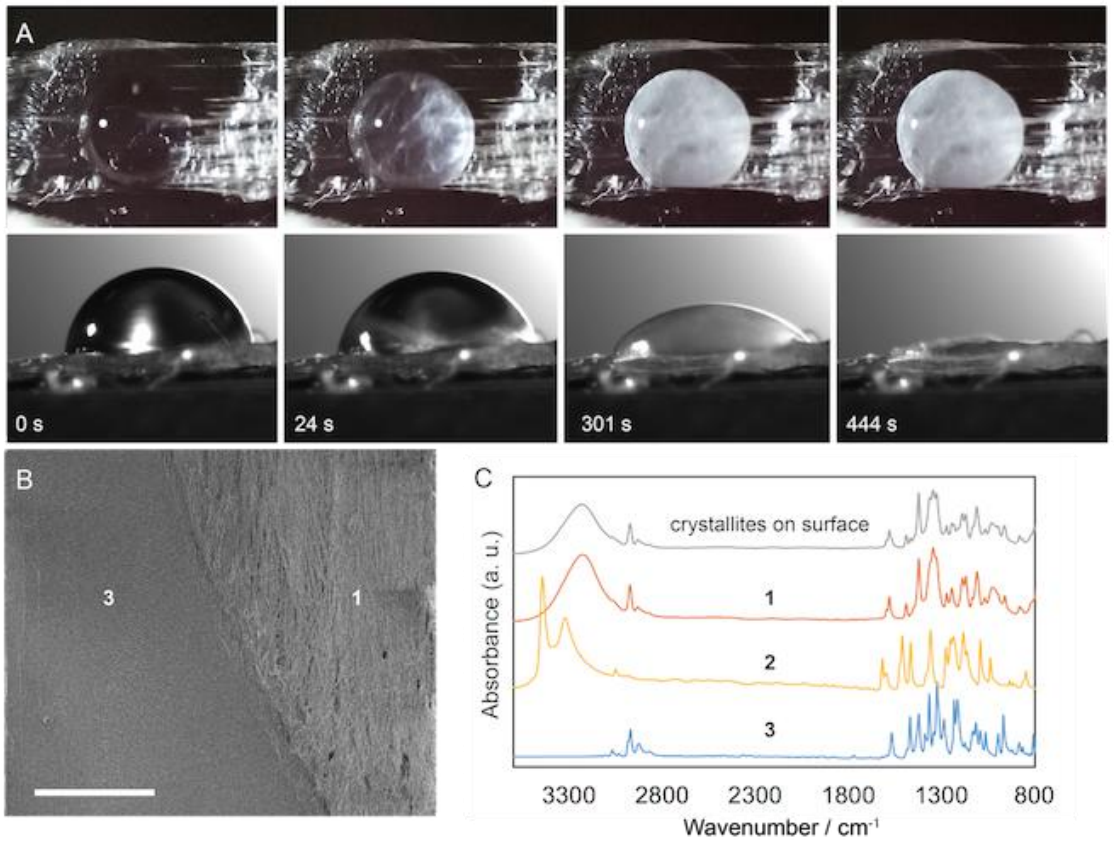

Fig. S7 Hydrolysis of **3** into **1** and **2** on the surface of the crystal. (a) A series of snapshots of a droplet of water reacting on the surface of crystal of **3** monitored simultaneously from two perspectives over 444 s. **3** rapidly reacts with water to form **1** and **2**. While **2** is soluble in water, **1** is not and it rapidly crystallizes inside the droplet as its concentration increases over time. (b) An SEM image of the surface **3** after water was drop-cast onto it. Both the unaffected surface (left) and the hydrolyzed surface containing the crystallites (right) are shown. Scale bar, 100 mm. (c) IR spectra of the resulting crystallites that were harvested from the surface and identified as **1** using IR spectroscopy. The IR spectra of **1**, **2** and **3** are shown for comparison.

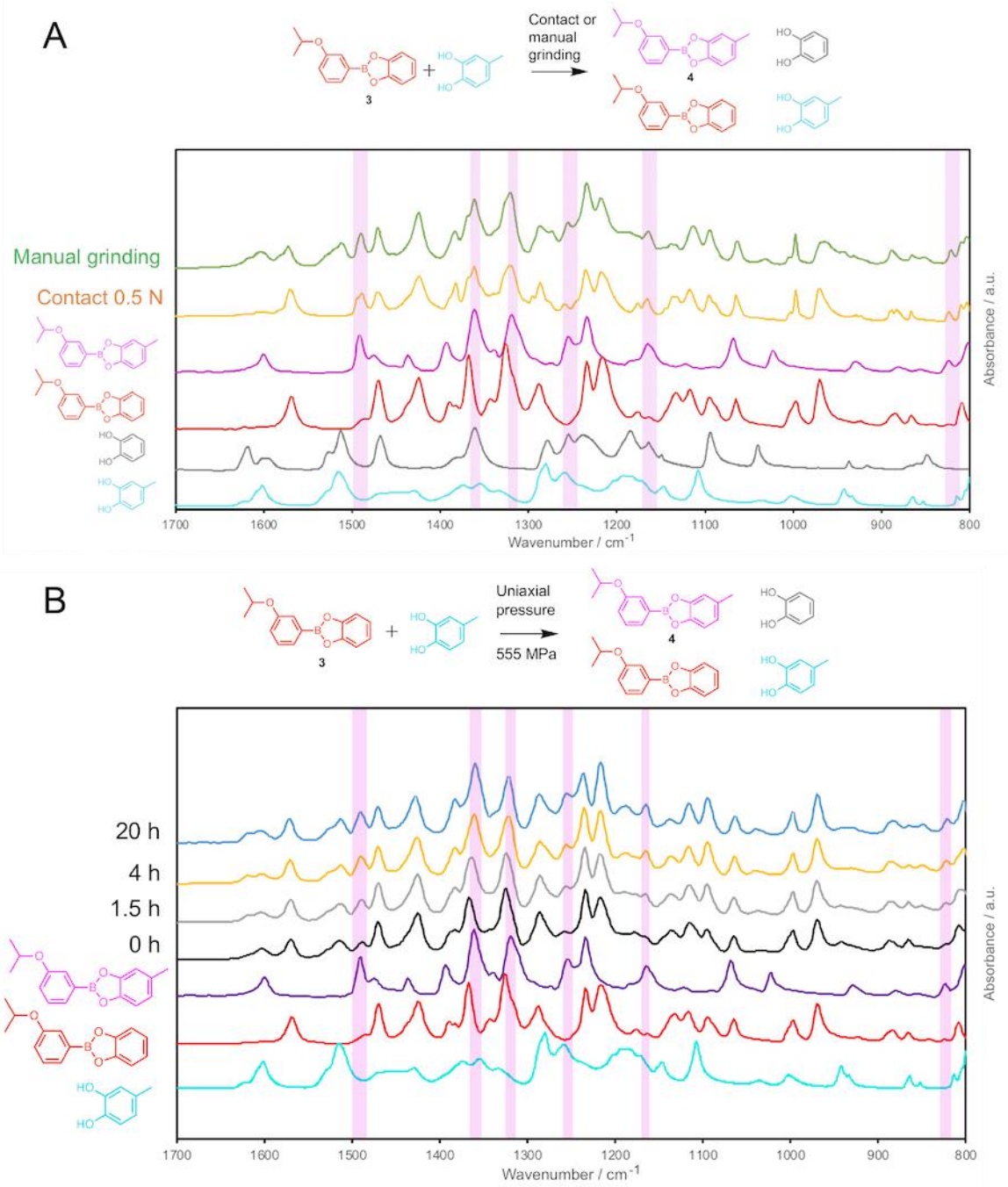

Fig. S8 ATR FT-IR spectra of **3** after being placed in contact, manually ground, and uniaxially pressed with 4-methylcatechol. (A) The sample was placed **3** in contact with 0.5 N of force with 4-methylcatechol for 16 h and then measured. A separate sample of **3** was also manually ground in a 1:1 molar ratio with 4-methylcatechol for 30 s and its spectrum was recorded. Both the contact and grinding experiments show the transesterification product **4**. (B) **3** was uniaxially pressed with 4-methylcatechol and the reaction was measured over 20 h. The peaks for the transesterification product **4** that are present on the surface of **3** are shown in magenta highlights.

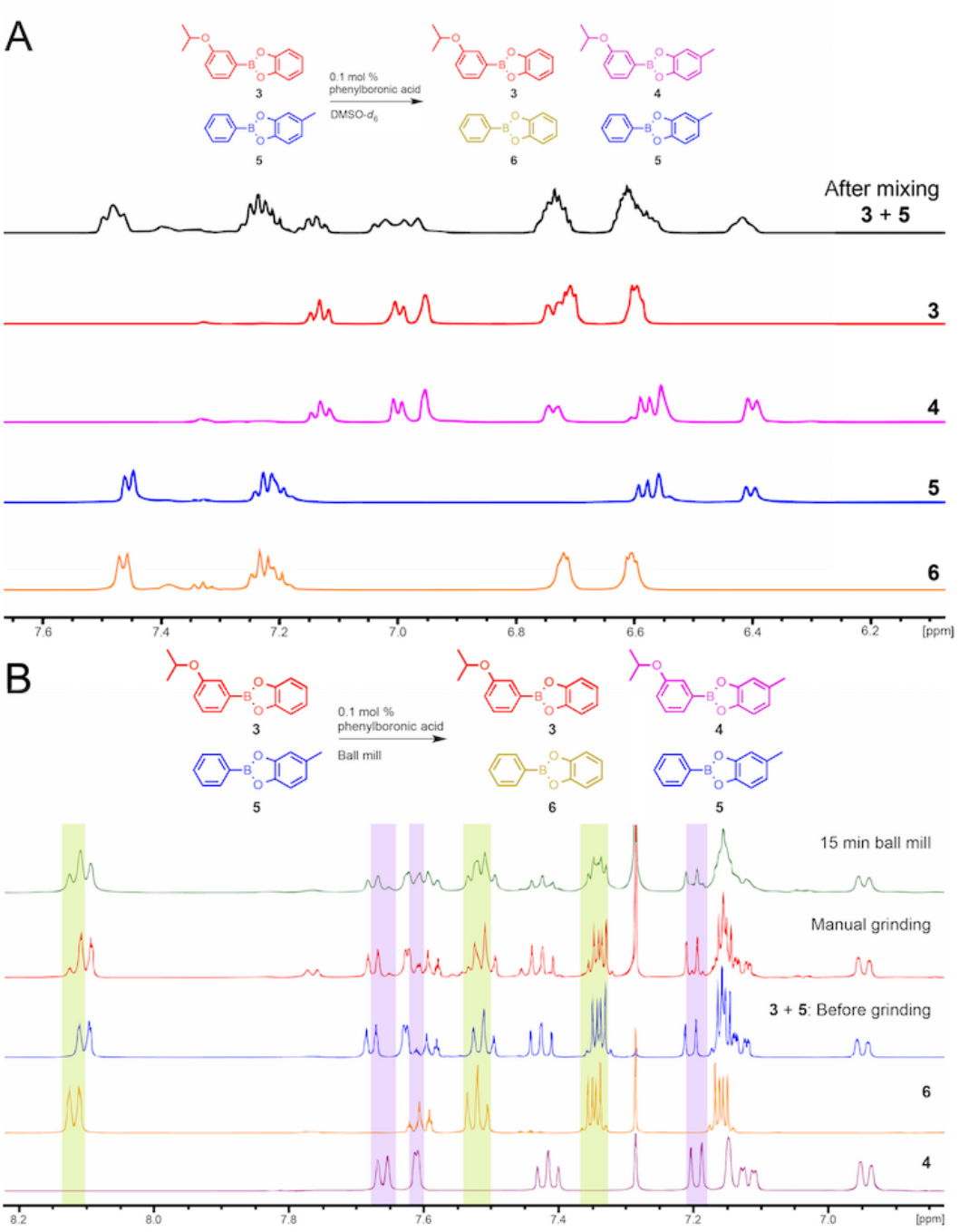

Fig. S9 The reaction of **3** and **5** in a solution of DMSO-d_6 and solid state monitored by ^{1}H NMR spectroscopy. (A) The metathesis reaction of mixing **3** and **5** in a solution. Spectral overlap and the broadness of the signal prevents quantification of the reaction, though the 1 : 1 ratio in the intensity of the peaks of the overlapped doublets at 6.4 and 7.5 ppm suggests the expected 1 : 1 : 1 : 1 ratio of **3** : **4** : **5** : **6**. (B) The solid state metathesis reaction was followed by first hand grinding the sample and then using a ball mill. The formation of **4** and **6** was observed as shoulders in the ^{1}H NMR spectrum after manual grinding and ball-milling and are highlighted in magenta and yellow, respectively. The spectra of pure **4** and **6** are shown for comparison.

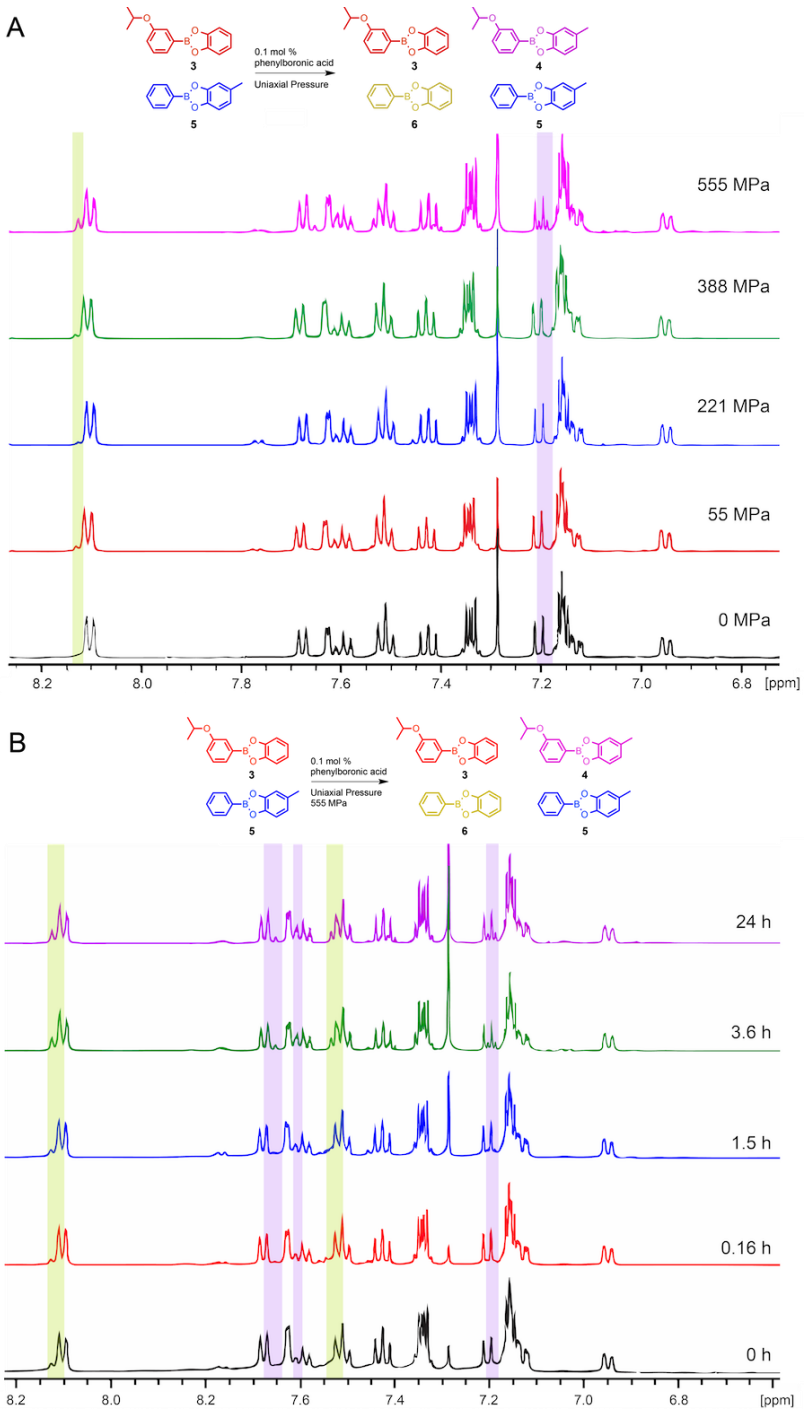

Fig. S10 The metathesis of **3** and **5** with 0.1% (mol) of phenylboronic acid using uniaxial pressure and monitored by the ^{1}H NMR in $CDCl_3$. (A) The metathesis reaction at a constant duration (4 h) and varying loads. The degree of boronic ester exchange increases with increasing pressure with final percent composition of 13% for **4** and **6** at 555 MPa. (B) The metathesis reaction at a constant load (555 MPa) and varying durations. The percent composition of the mixture increases from 8, 12, 11, 12, 13% for **4** and 6, 9, 13, 13, 13% for **6** after 0, 0.16, 1.5, 3.6 and 24 h, respectively. The peaks from **4** at 7.2 ppm and **6** at 8.13 ppm are highlighted in purple and yellow, respectively.

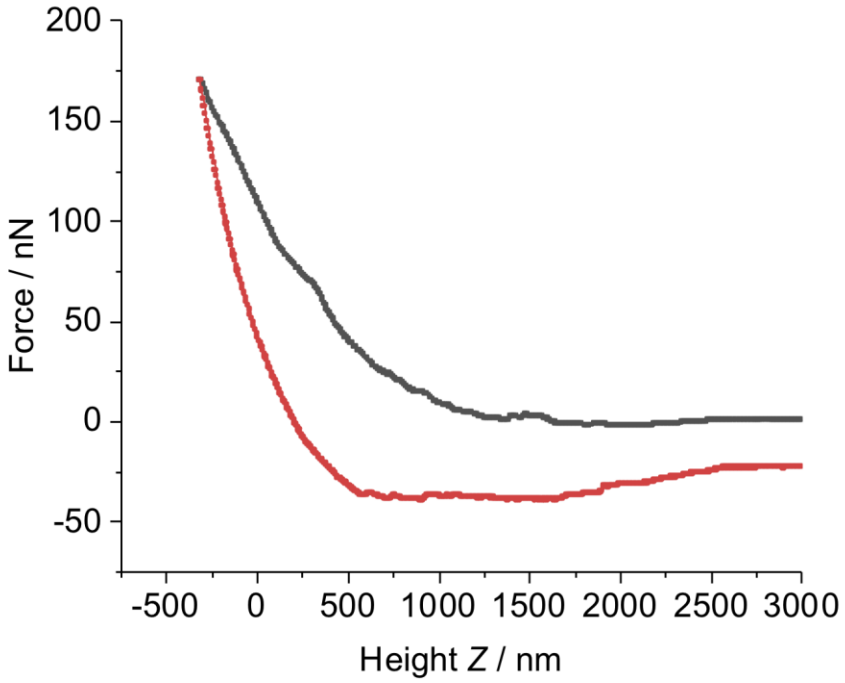

Fig. S11 A representative adhesion force curve between a cantilever mounted with a crystal of **3** and a sapphire surface. The adhesion force was found to be -39.77 ± 2.39 nN over three measurements.

Table S1 Three-point bending tests on five crystals of **3.**

Crystal	Width (mm)	Thickness (mm	Length (mm)	Elastic Moduli (MPa)
A	0.877	0.337	2.1	4.8
B	0.721	0.368	2.1	6.7
C	0.487	0.298	2.1	5.8
D	0.506	0.231	2.1	27.15
E	0.637	0.281	2.1	15.8

Table S2 Crystallographic parameters of compound **3.**

Temperature / K	100 K
Radiation source	Mo
Formula weight	254.1
Crystal system	Monoclinic
Space group	$P2_1/c$
a / Å	24.5290(24)
b / Å	4.5725(4)
c / Å	12.2240(11)
α / °	90
β / °	103.256(3)
γ / °	90
Volume / Å^3	1334.50(10)
Z	4
Density / (g cm^{-3})	1.26
μ / mm^{-1}	0.086
F_{000}	536
h_{min}, h_{max}	–27, 29
k_{min}, k_{max}	–5, 5
l_{min}, l_{max}	–14, 14
No. of measured reflections	17045
Crystal Mosaicity	0.58°
No. of unique reflections	2343
No. of reflections used	2255
R_{all}, R_{obs}	0.071, 0.069
$wR_{2,all}$, $wR_{2,obs}$	0.154, 0.153
$\Delta\rho_{min,max}$ / (e Å^{-3})	-0.336, 0.250
GooF	1.332
CCDC No.	1828493

Table S3. Adhesion force between a crystal of **3** and a surface of **3**.

Exp #	**Max Adhesion Force (nN)**
1	-56.31
2	-56.08
3	-53.95
4	-56.63
5	-55.07
6	-59.60
7	-58.37
8	-55.70
9	-56.01
10	-54.73
11	-55.19
12	-55.98
13	-57.22
14	-58.49
15	-56.92
Mean	**-56.42**
SD	**1.52**

Table S4. Adhesion force between a crystal of **3** and a sapphire surface.

Exp #	**Max Adhesion Force (nN)**
1	-37.78
2	-42.42
3	-39.1
Mean	**-39.77**
SD	**2.39**

Legends to the Supplementary Movies

Movie 1. Three-point bending of a crystal of **3** on the (100) face of the crystal.

Movie 2. Unbending and straightening of a mechanically bent crystal of **3.**

Movie 3. Elastic recovery of the shape of a crystal of **3** during twisting.

Movie 4. Twisting of a crystal of **3** around its long axis (in the [001] direction) up to 1080° using a miniature torque-transducing device. The movie is played at twice the original speed.

Movie 5. The repeated coiling and uncoiling of a crystal of **3** around a glass capillary. The movie is played at twice the original speed.

Movie 6. A computerized tomography (CT) scan of a crystal of **3** that was joined at opposite ends to form a ring-shaped object. The bottom portion of the crystal was mounted using molding clay and is not shown.

Movie 7. The breaking of **3** by applying force to the (10 $\overline{2}$) face of the crystal.

Movie 8. A 3D representation of the molecular mechanism of bending of a crystal of **3**.

Movie 9. A 3D representation of the molecular mechanism of breaking of a crystal of **3**.

Movie 10. A 3D representation of the molecular mechanism of twisting of a crystal of **3**.

Movie 11. A cross-sectional computerized tomography (CT) scan of a crystal of **3** before compression.

Movie 12. A cross-sectional computerized tomography (CT) scan of a healed crystal of **3** after compression.

Movie 13. Time-lapsed atomic force microscopy images of a surface on the (100) face of a crystal of **3** recorded over 18.5 hours.

^{1}H and ^{13}C nuclear magnetic resonance and infrared spectroscopy of all new compounds

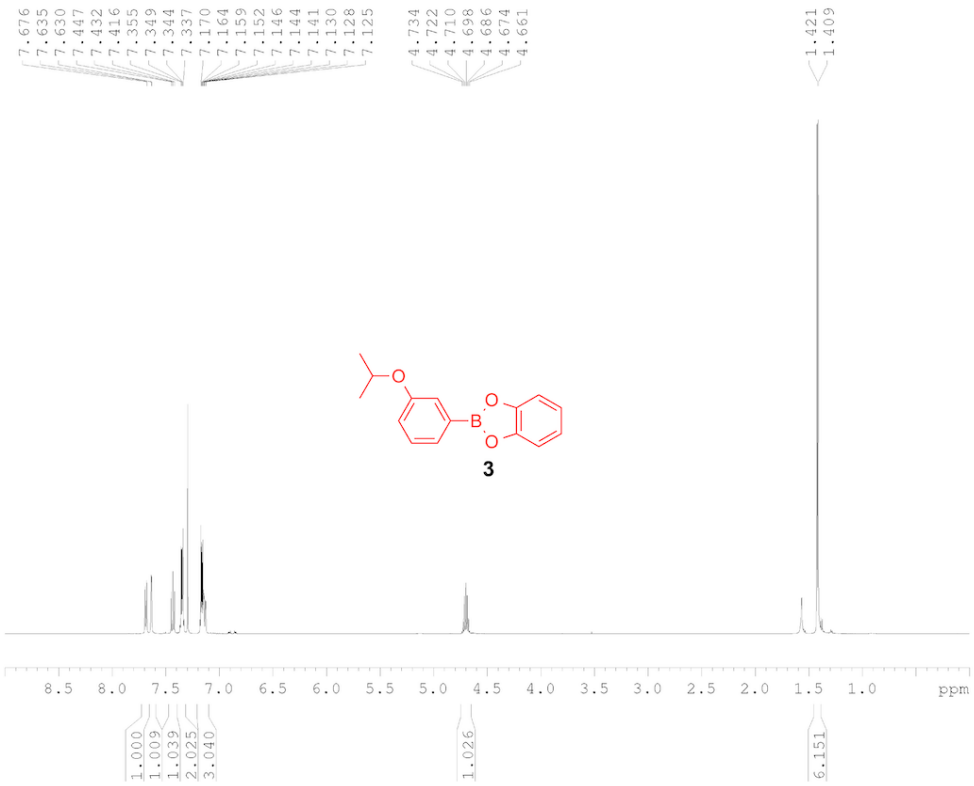

^{1}H NMR (500 MHz) of 3 in $CDCl_3$. Small amounts of catechol and 3-isopropoxyphenyl boronic acid are present due to hydrolysis from ambient water.

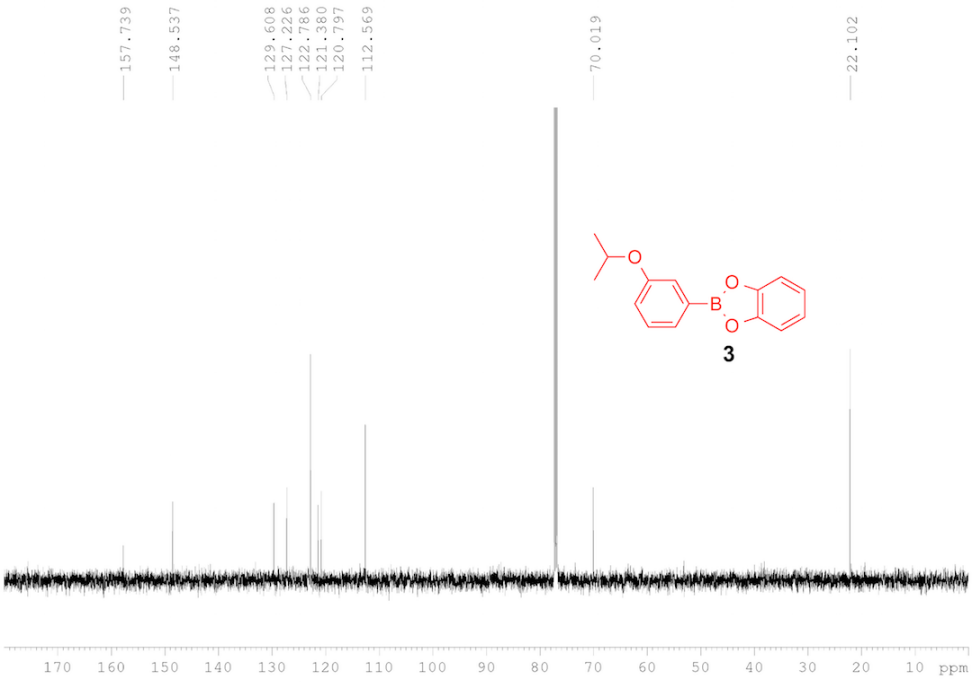

^{13}C NMR (125 MHz) of 3 in $CDCl_3$.

\\\\\\\\\

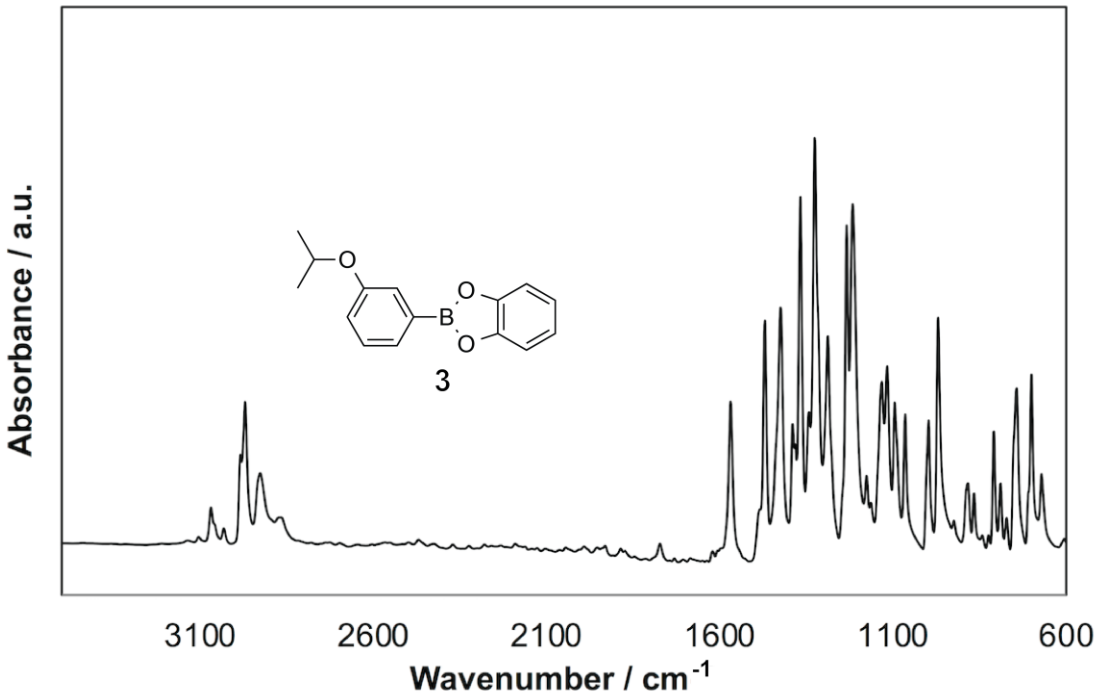

ATR-FTIR spectrum of 3 in the solid.

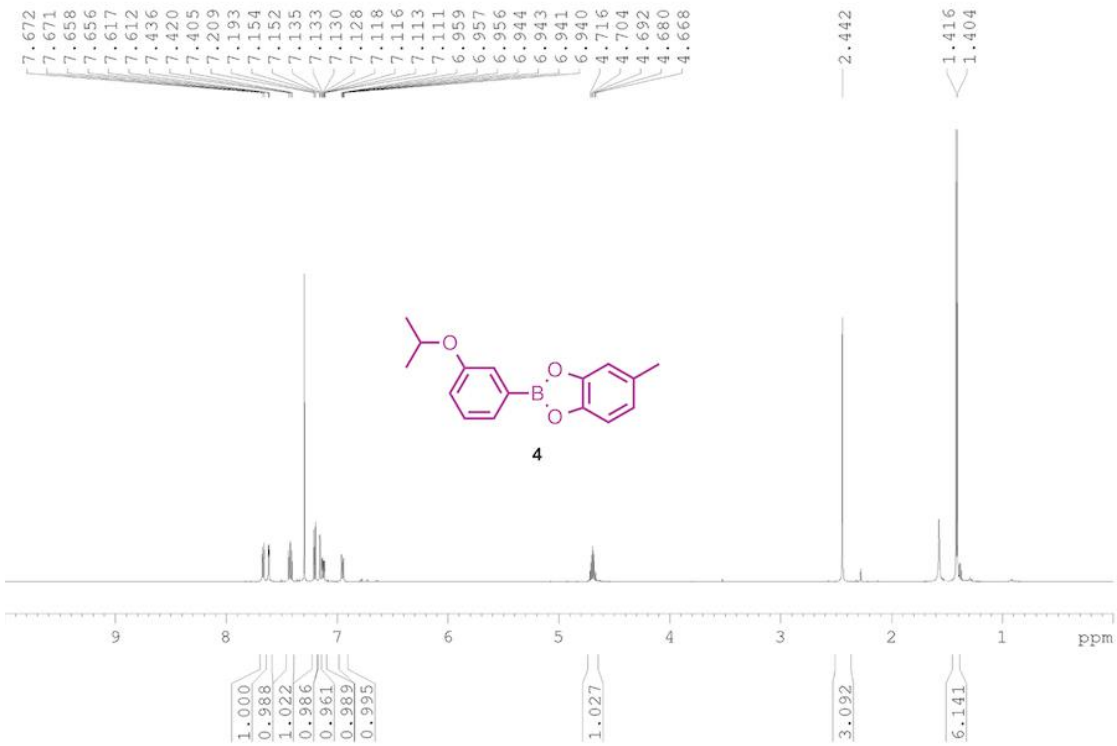

^{1}H NMR (500 MHz) of 4 in $CDCl_3$. Small amounts of 4-methylcatechol and 3-isopropoxyphenyl boronic acid are present due to hydrolysis from ambient water.

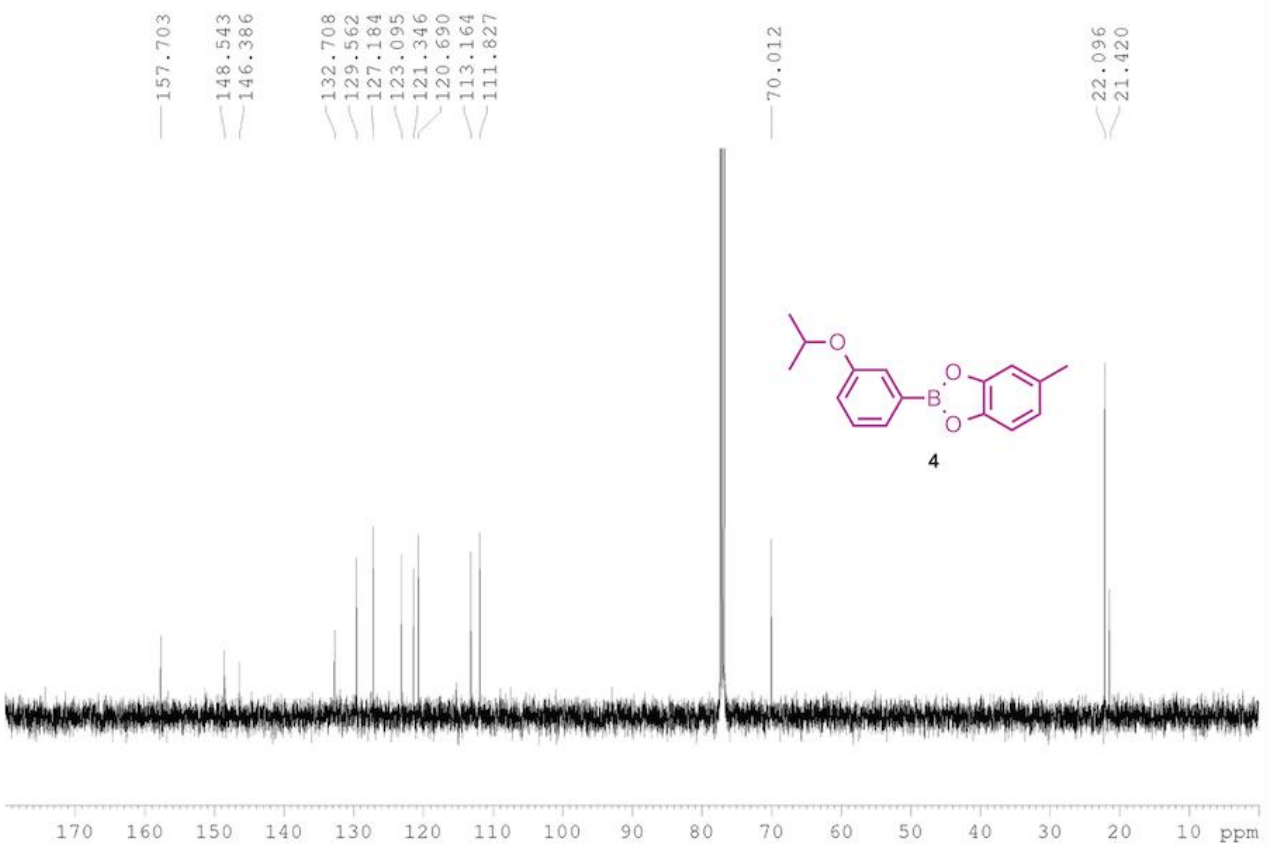

^{13}C NMR (125 MHz) of 4 in $CDCl_3$.

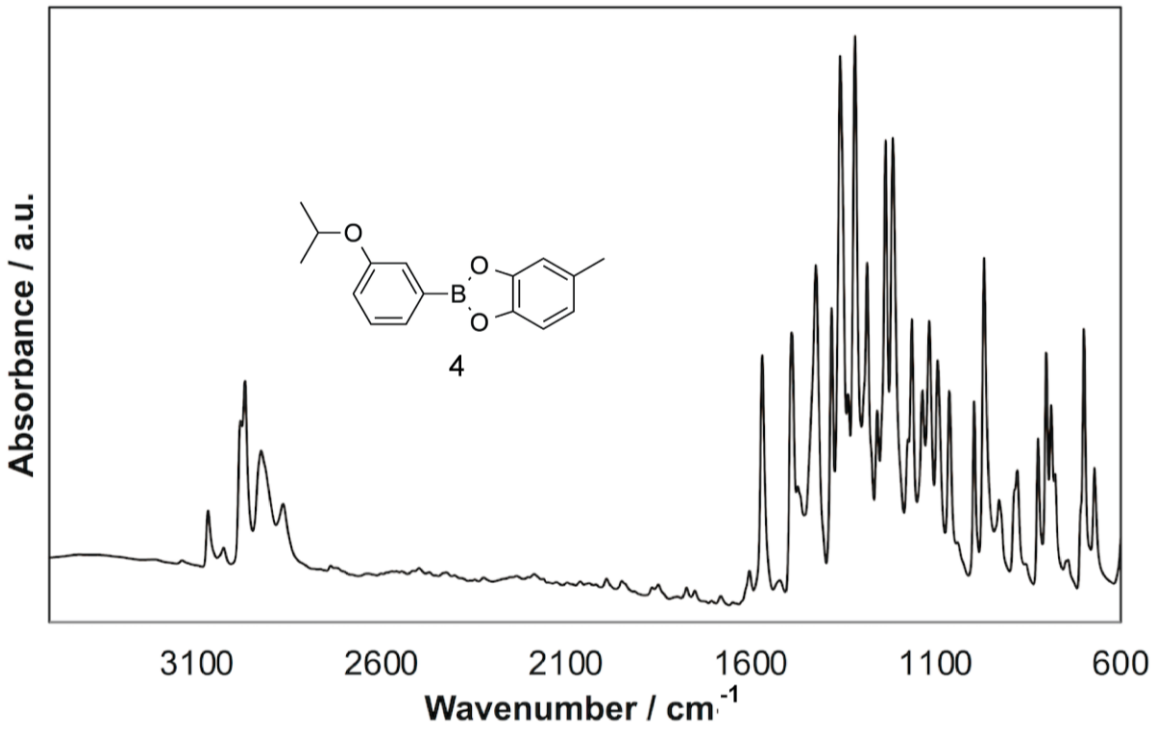

ATR-FTIR spectrum of 4 in the solid.

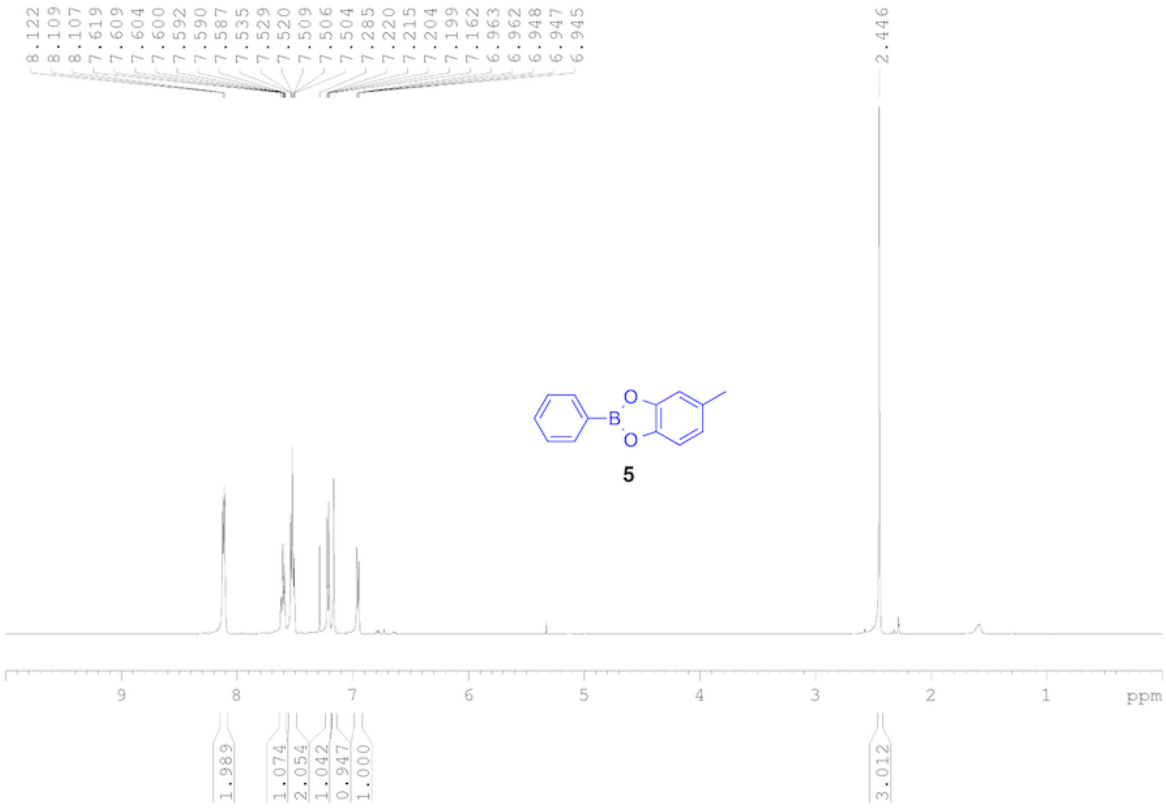

^{1}H NMR (500 MHz) of 5 in $CDCl_3$. Small amounts of 4-methylcatechol and phenyl boronic acid are present due to hydrolysis from ambient water.

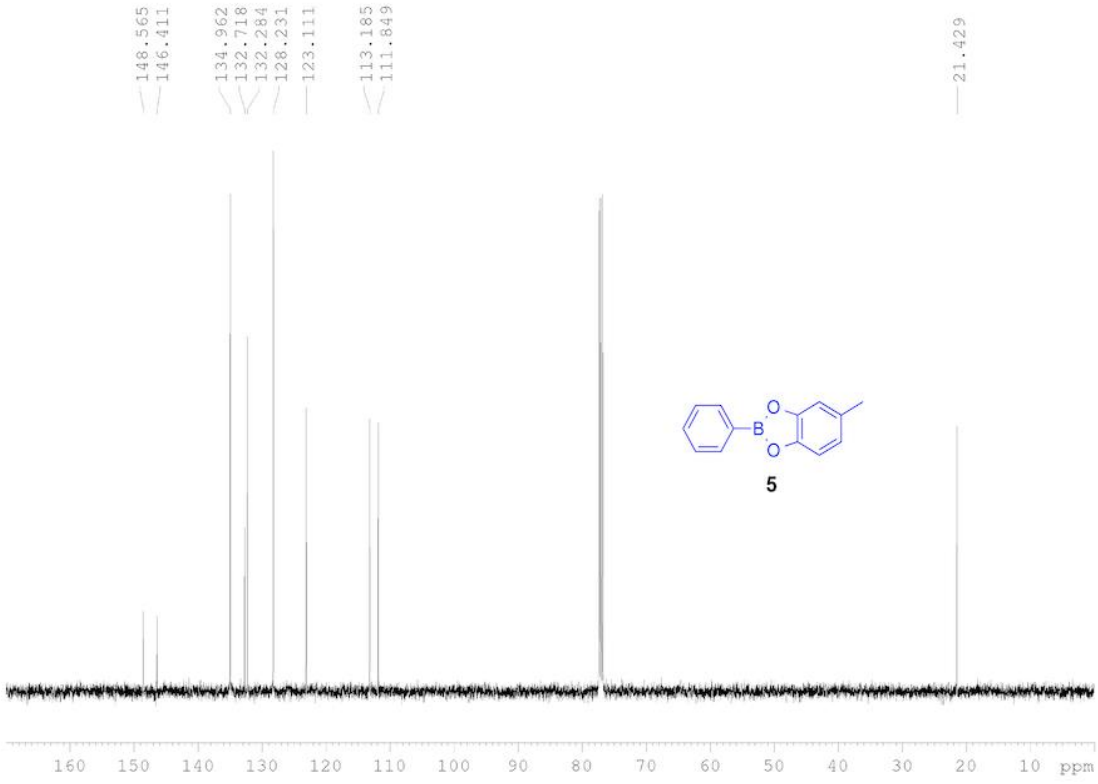

^{13}C NMR (125 MHz) of 5 in $CDCl_3$.

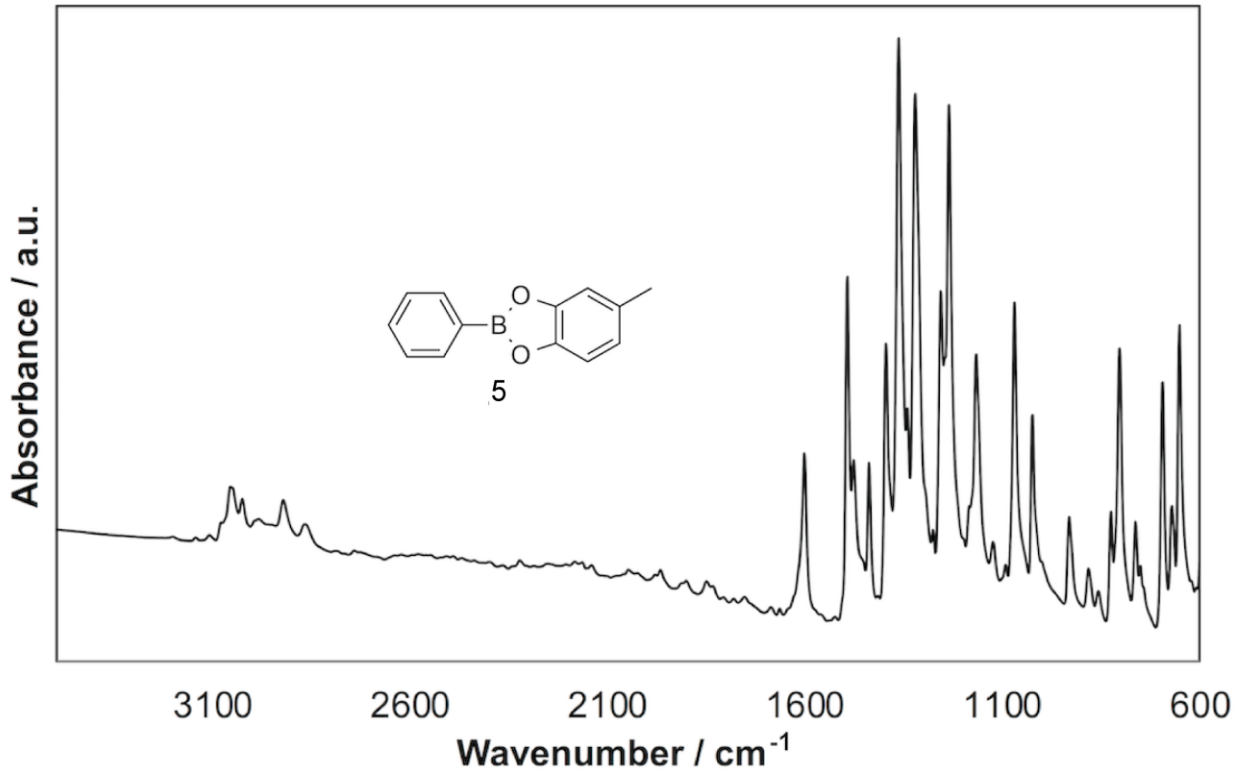

ATR-FTIR spectrum of **5** in the solid.